ADVANCED FUNCTIONAL MATERIALS

Supporting Information

for *Adv. Funct. Mater.*, DOI: 10.1002/adfm.201901388

Thermally Conductive Reduced Graphene Oxide Thin Films for Extreme Temperature Sensors

*Yuqiang Zeng, Tian Li, Yonggang Yao, Tangyuan Li, Liangbing Hu, and Amy Marconnet**

Supporting Information

Thermally Conductive Reduced Graphene Oxide Thin Films for Extreme Temperature Sensors

*Yuqiang Zeng, Tian Li, Yonggang Yao, Tangyuan Li, Liangbing Hu, and Amy Marconnet**

Note S1 | Preparation of RGO films

An aqueous GO solution is prepared with an improved Hummer's method[1,2] and 3D printed to form uniform films. Details of 3D printing of GO films can be found in prior work.[3] A two-step annealing process reduces the GO films to RGO films.[3–5] First, the GO films are annealed at 1000 K in a tube furnace under argon atmosphere and obtain good uniformity and electrical conductivity. Then, they are Joule heated to further thermally reduce the GO leveraging the high melting point of carbon-based materials. Specifically, they are gradually Joule-heated to 2000 K or 3000 K for this work, and even higher temperatures are possible with increasing electrical input. An example of a free-standing electrically heated GO film at 2300 K in vacuum is shown in Figure 1(a-c). The temperature during Joule heating is determined by fitting the emitted radiation spectrum to the Planck distribution $I_\lambda(\lambda,T)=\frac{2hc^2}{\lambda^5\exp(hc/(\lambda k_B T-1))}$, where h, c, k_B, and λ are the Planck constant, speed of light in vacuum, Boltzmann constant, and wavelength, respectively. The emission intensity of the Joule heated RGO films is measured by a fiber-coupled spectrometer (Ocean Optics. Inc.). Although the ends of the sample are significantly colder, a large portion near the center of the sample achieves the desired annealing temperature.

Note S2 | Characterizations of RGO films

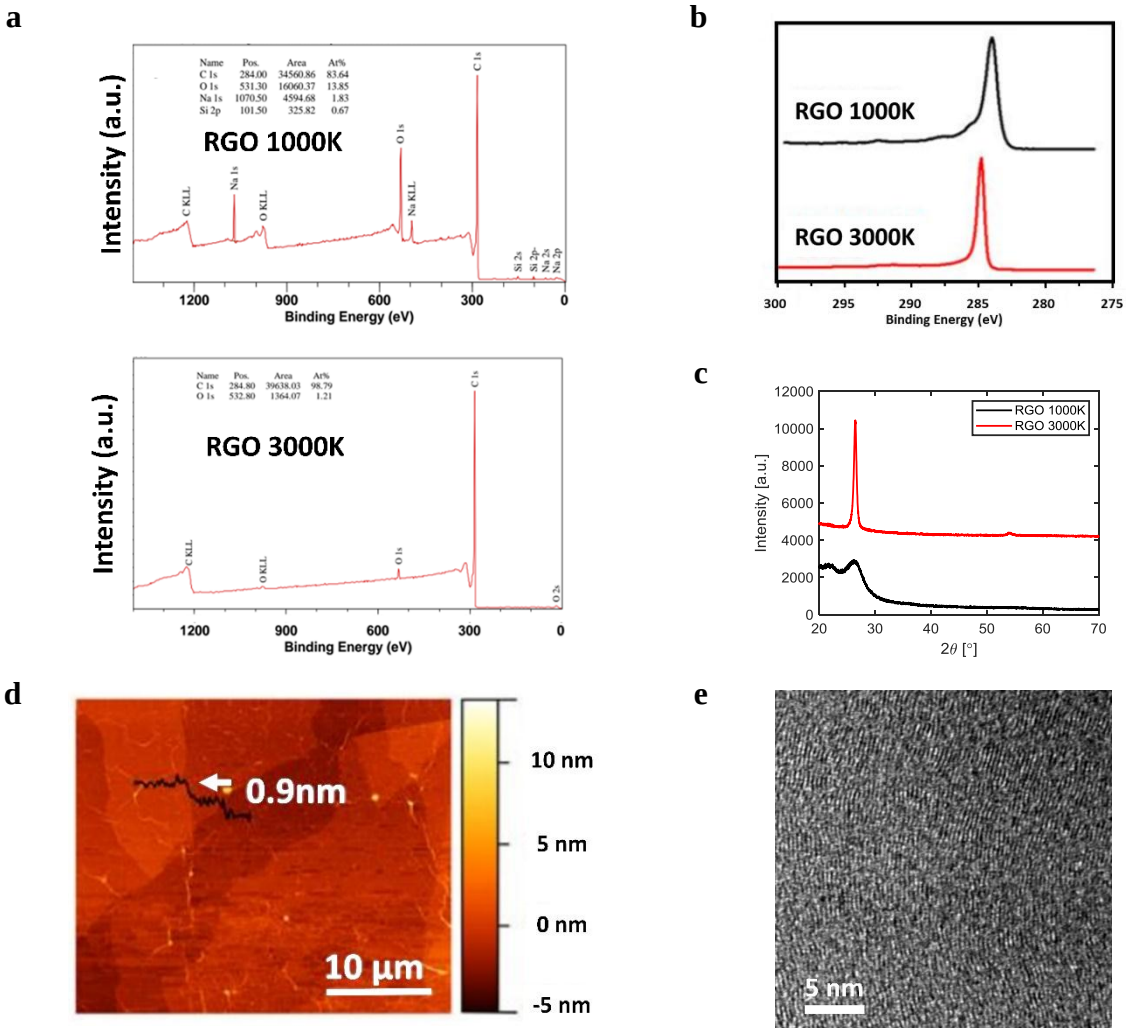

Figure S1. a) XPS data of RGO 1000K and RGO 3000K, respectively. The atomic ratio of carbon to oxygen increases from 6.04 in RGO 1000K to 81.64 in RGO 3000K, and impurities are further removed after annealing at 3000 K. b) The narrower full width at half maximum of RGO 3000K, when compared to RGO 1000K, confirms the improved crystallinity in RGO films reduced at 3000 K. c) XRD data of RGO 1000K and RGO 3000K. The relative position of the characteristic peak between RGO 1000K and RGO 3000K indicates the decrease of the layer-layer distance in RGO films when annealed at higher temperatures. The narrow and sharp characteristic peak in RGO 3000K corresponds to the increased size of ordered graphitic sp^2 domains due to the sp^3-to-sp^2 bond conversion at high temperature annealing. d) Monolayer RGO nanosheets in RGO 3000K by atomic force microscopy. e) TEM image of RGO 3000K shows its crystalline graphene-like structure. The scale bar is 5 nm. Panel (b) and (d) reproduced with permission from our previous work.[5]

Note S3 | Electrothermal measurements

Assuming negligible convective and radiative heat loss, the governing equation for one-dimensional heat conduction in the suspended RGO film is

$$kA\frac{d^2T}{dx^2} + I^2\frac{R_0}{L} = 0 \text{ and} \qquad (1)$$

$$T(\pm\frac{L}{2}) = T_0, \qquad (2)$$

where k is the thermal conductivity of the RGO film, I is the applied electrical current, R_0 is the electrical resistance at the stage temperature T_0, A is the cross-section area, and L is the length of the suspended RGO film. Note that resistance variation with temperature is sufficiently small compared to R_o, *e.g.*, $|\Delta R/R_0| < 0.5\%$ for a temperature rise ~10 K by Joule heating at 300 K, the Joule heating term here neglects the secondary effect of the decreasing electrical resistance with temperature. This differential equation can be solved analytically, and the analytical solution of the temperature is

$$\Delta T(x) = T(x) - T_0 = -\frac{I^2R_0}{2kAL}x^2 + \frac{I^2R_0L}{8kA}. \qquad (3)$$

The thermal conductivity is derived from the measured power and average temperature rise as

$$k = \frac{I^2R_0L}{12A\int_{-L/2}^{L/2}\Delta T(x)dx/L} = \frac{I^2R_0L}{12A\Delta\overline{T}}. \qquad (4)$$

The average temperature rise of the self-heating RGO film is determined using a calibrated relationship between the electrical resistance and temperature. For the calibration at each stage temperature, we sweep the current in a small range (~10^{-5} A) and extract the electrical resistance corresponding to the stage temperature from the slope of the I-V curve. The current is limited to this small value during calibration to minimize the temperature rise due to Joule heating: the temperature profile of a Joule heated film in vacuum is parabolic based on the one-dimensional analytical solution. The exact maximum temperature rise during the calibration is determined after the calibration process is completed for the whole temperature

range. The verified temperature rise during the calibration (< 0.1 K) is sufficiently small compared to the temperature rise used for the measurement of thermal conductivity (~10 K), that the temperature of the stage can be used along with the measured resistivity during calibration to determine the temperature-dependent resistivity. Thus, the temperature in Figure 2(b) is the stage temperature (as the temperature rise of the film during the calibration is <0.1 K).

During the thermal conductivity tests, the current is increased beyond the calibration range (~ 10^{-3} A) leading to a more significant temperature rise within the film. Thus, when the resistance is measured as a function of current (at a particular stage temperature such as shown in Figure 2c), the change in resistance can be converted to an average temperature rise within the sample film. Thus, in Figure 2d, the temperature is an average across the heated film, which is determined from the measured electrical resistance with the calibrated relationship between the resistance and temperature.

Note S4 | Mott variable-range hopping (Mott-VRH) models

To understand the electrical transport mechanism, we fit the temperature-dependent electrical conductivity of RGO films with multiple VRH models:[6] 1) VRH model, 2) VRH model combined with quantum tunneling (VRH & Q-T), and 3) VRH model combined with quantum tunneling and thermal activation (VRH & Q-T & T-A). The fitting is done with a nonlinear least-squares solver (*lsqcurvefit*) in MATLAB. The fitting results suggest that the third model fully explains the electrical transport in RGO films annealed at different temperatures. The first model explains well the experimental data of RGO 1000K at high temperature but deviates from the data at low temperature. Further, the first model cannot capture the temperature dependence of RGO 2000K and RGO 3000K. Fitting to the experimental data with the second model is reasonably good, but deviations are observed at low temperature.

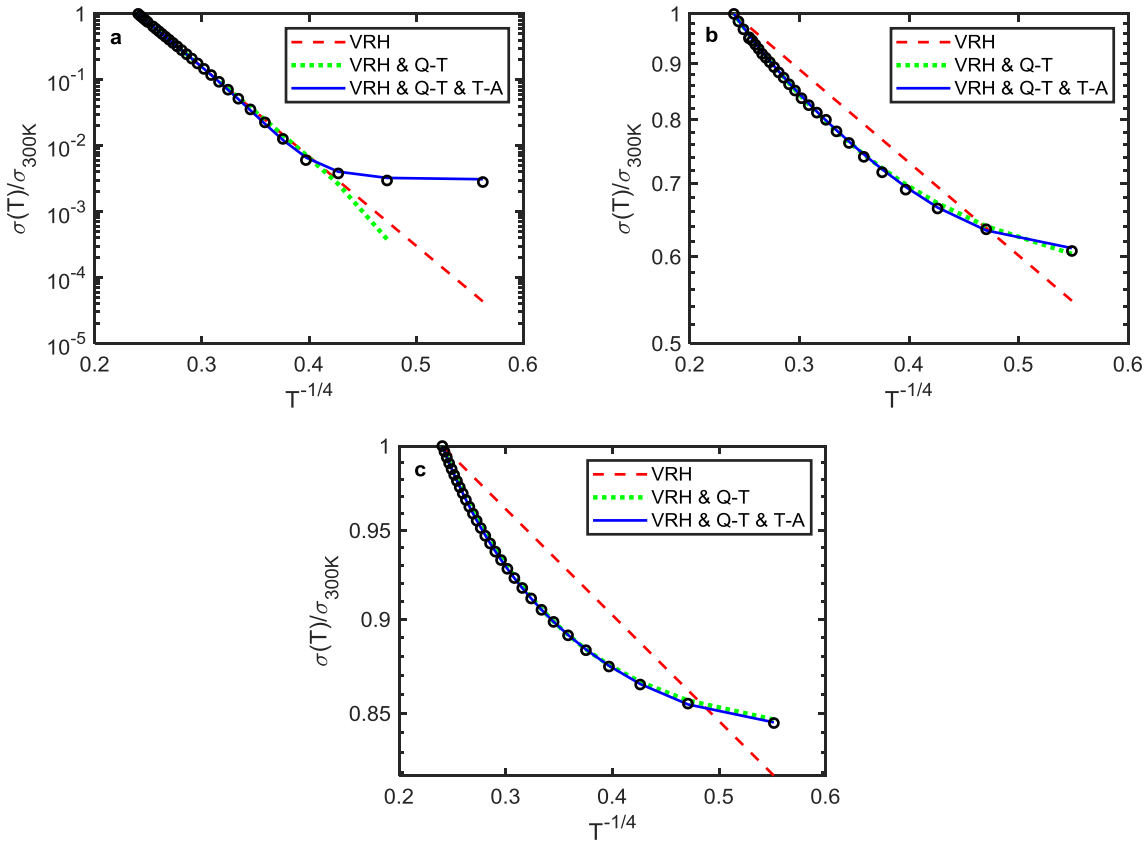

Figure S2. Normalized electrical conductivity $\sigma(T)/\sigma_{300\ K}$ of a) RGO 1000K, b) RGO 2000K, and c) RGO 3000K as a function of $T^{-1/4}$. The electrical conductivity data is fit with multiple VRH models. The fitting results suggest that the VRH model combined with

quantum tunneling and thermal activation fully explains the electrical transport in RGO films annealed at different temperatures.

Table S1. Fitting parameters of multiple VRH models

	VRH		VRH & Q-T			VRH & Q-T & T-A				
	$G_h(mS)$	$H(K^{1/4})$	$G_h(mS)$	$H(K^{1/4})$	$G_t(mS)$	$G_h(mS)$	$H(K^{1/4})$	$G_a(mS)$	$T_a(K)$	$G_t(mS)$
RGO 1000K	398.5	31.2	396.0	31.2	0	1238.5	36.9	0.1	241.8	0.0007
RGO 2000K	17.5	2.0	28.6	7.2	6.3	64.9	13.9	2.5	48.9	6.8
RGO 3000K	28.5	0.6	38.7	9.4	20.9	79.0	13.9	1.3	39.2	21.0

Note S5 | Stability and repeatability of RGO 3000K

To demonstrate the stability and repeatability of RGO 3000K for temperature sensing, we perform current-voltage (I-V) sweep measurements for RGO 3000K at three representative temperatures, i.e., 10 K for low temperature, 300 K for room temperature, and 925K for high temperature. The same I-V sweep is performed after one week and two weeks, respectively. A good agreement of the I-V curve is observed for all the temperatures between the first measurement and the repeated tests (see Figure S3a-c). The minimal resistance variation (within ±3%) after two weeks verifies the stability and repeatability of our RGO 3000K at low and high temperatures. Further, for the extremely high-temperature range, Figure S3d shows that the resistance variation of RGO 3000K is less than 5% after 50h continuous operation around 2460 K, which indicates its good stability at such an extreme temperature.

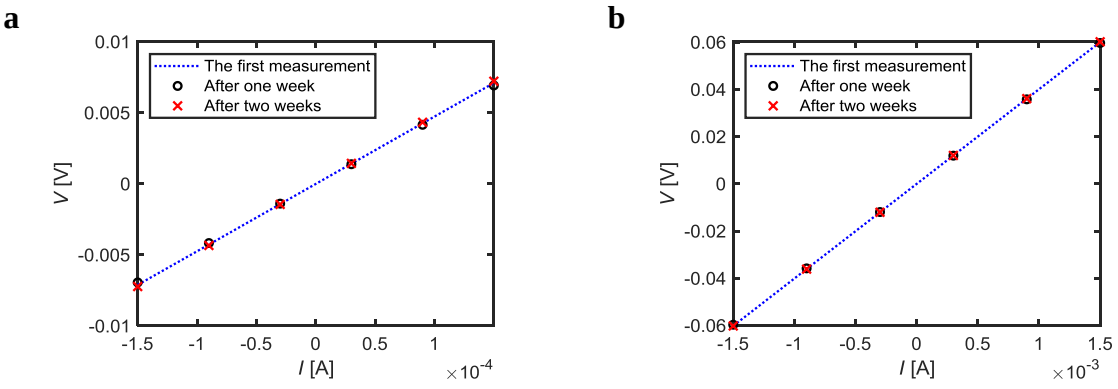

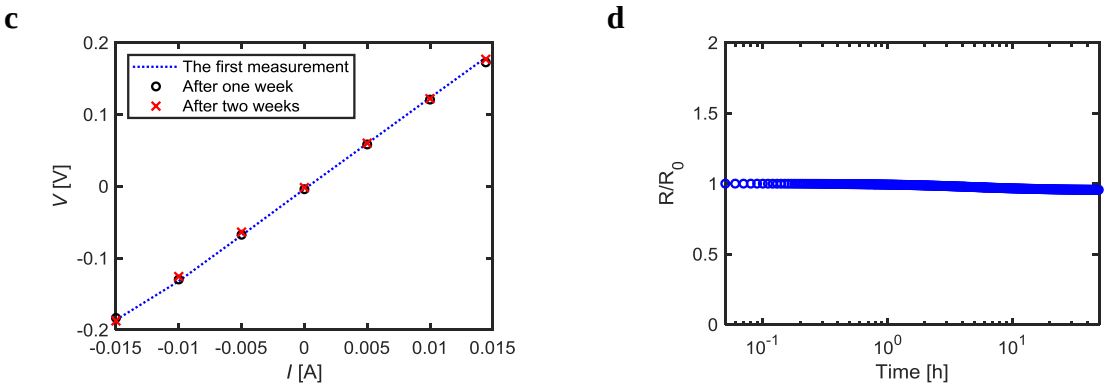

Figure S3. The I-V characteristic of RGO 3000K at a) 10 K, b) 300 K, and c) 925 K. A good agreement of the I-V curve is observed between the first measurement and the repeated tests after one week and two weeks, respectively. The resistance variation in two weeks is within ±3% for all cases, which verifies the stability and repeatability of our RGO 3000K at low and high temperatures. d) The resistance variation of RGO 3000K at an extremely high temperature (~2460 K). The slight resistance variation (< 5%) after 50 h continuous operation verifies its stability at such an extreme temperature. Panel (d) reproduced with permission from our previous work.[5]

Table S2. Comparison of the response of RGO 3000K, Pt, and Cu for temperature sensing

	Temperature sensitivity $\|d\rho/dT\|$ at 300K (μΩ*cm/K)	Dynamic Range (*dB*)	Normalized Response time at 300K	Stability
RGO 3000K	0.2305	24.77	1	Good
Pt	0.0416	14.64	4.2	Good
Cu	0.0068	8.07	0.9	Poor

References

[1] W. S. Hummers, R. E. Offeman, *J. Am. Chem. Soc.* **1958**, *80*, 1339.
[2] D. C. Marcano, D. V Kosynkin, J. M. Berlin, A. Sinitskii, Z. Sun, A. Slesarev, L. B. Alemany, W. Lu, J. M. Tour, *ACS Nano* **2010**, *4*, 4806.
[3] W. Bao, A. D. Pickel, Q. Zhang, Y. Chen, Y. Yao, J. Wan, K. Fu, Y. Wang, J. Dai, H. Zhu, D. Drew, M. Fuhrer, C. Dames, L. Hu, *Adv. Mater.* **2016**, 4684.
[4] Y. Chen, K. Fu, S. Zhu, W. Luo, Y. Wang, Y. Li, E. Hitz, Y. Yao, J. Dai, J. Wan, V. A. Danner, T. Li, L. Hu, *Nano Lett.* **2016**, *16*, 3616.
[5] T. Li, A. D. Pickel, Y. Yao, Y. Chen, Y. Zeng, S. D. Lacey, Y. Li, Y. Wang, J. Dai, Y. Wang, B. Yang, M. S. Fuhrer, A. Marconnet, C. Dames, D. H. Drew, L. Hu, *Nat. Energy* **2018**, *3*, 148.
[6] H.-J. Kim, D. Kim, S. Jung, S. N. Yi, Y. J. Yun, S. K. Chang, D. H. Ha, *J. Phys. Chem. C* **2015**, *119*, 28685.